

The Sunyaev–Zel’dovich temperature of the intracluster medium

Scott T. Kay,^{1*} Leila C. Powell,² Andrew R. Liddle³ and Peter A. Thomas³

¹*Jodrell Bank Centre for Astrophysics, School of Physics and Astronomy, The University of Manchester, Manchester M13 9PL*

²*Astrophysics, University of Oxford, Keble Road, Oxford OX1 3RH, UK*

³*Astronomy Centre, Department of Physics and Astronomy, University of Sussex, Brighton BN1 9QH, UK*

This draft was generated on 7 March 2008

ABSTRACT

The relativistic Sunyaev–Zel’dovich (SZ) effect offers a method, independent of X-ray, for measuring the temperature of the intracluster medium (ICM) in the hottest systems. Here, using N -body/hydrodynamic simulations of three galaxy clusters, we compare the two quantities for a non-radiative ICM, and for one that is subject both to radiative cooling and strong energy feedback from galaxies. Our study has yielded two interesting results. Firstly, in all cases, the SZ temperature is hotter than the X-ray temperature and is within ten per cent of the virial temperature of the cluster. Secondly, the mean SZ temperature is less affected by cooling and feedback than the X-ray temperature. Both these results can be explained by the SZ temperature being less sensitive to the distribution of cool gas associated with cluster substructure. A comparison of the SZ and X-ray temperatures (measured for a sample of hot clusters) would therefore yield interesting constraints on the thermodynamic structure of the intracluster gas.

Key words: hydrodynamics - methods: numerical - X-rays: galaxies: clusters

1 INTRODUCTION

Currently, nearly all of our knowledge of the intracluster medium (ICM) comes from X-ray observations, with the latest generation of X-ray satellites, *XMM-Newton* and *Chandra*, being capable of spatially resolving the density and temperature structure independently in low-redshift clusters out to tens of per cent of their virial radii (e.g. Arnaud, Pointecouteau & Pratt 2005; Vikhlinin et al. 2005; Pratt et al 2007). Separate density and temperature information is vital for probing the effects of physical processes (such as galactic outflows) on the structure of the ICM (e.g. from the entropy and pressure profiles), as well as for constructing mass–observable relationships for use in cosmological analyses. The latter is currently being driven by X-ray surveys such as the *XMM* Cluster Survey (Romer et al. 2001; Stanford et al. 2006), promising to find many new clusters out to redshifts $z > 1$.

The ICM is also detectable at centimetre and millimetre wavelengths through the Sunyaev–Zel’dovich (SZ) effect (Sunyaev & Zel’dovich 1972), the Inverse Compton scattering of cosmic microwave background (CMB) photons off free electrons in the ICM. As the SZ effect is a scattering process,

the observed SZ signal is independent of cluster redshift. Thus, thousands of new high-redshift clusters are promised from upcoming SZ surveys such as that to be performed by the South Pole Telescope (Ruhl et al. 2004).

For most clusters, the SZ effect will only measure the integrated pressure of the electrons along the line of sight, and so its use as a probe of ICM structure will be limited without additional X-ray data. The combination of SZ and X-ray surface brightness profiles yields a promising new way of obtaining cluster temperature information without having to resort to expensive X-ray spectroscopy; such a method yields a temperature that is closer to the mass-weighted temperature of the cluster (Ameglio et al. 2007).

It is possible, however, to measure the temperature of the ICM directly in the hottest clusters with multi-frequency SZ observations alone, due to significant relativistic effects in these systems (e.g. Rephaeli 1995; Stebbins 1997; Itoh et al. 1998; Challinor & Lasenby 1998; Pointecouteau, Giard & Barret 1998). In contrast to the above, this estimate of the temperature (hereafter referred to as the *SZ* temperature) is weighted by the pressure of the electrons along the line of sight. How the SZ and X-ray temperature measurements differ systematically, from a theoretical perspective, is the subject of this short paper. Here, using N -body/hydrodynamic simulations of galaxy clusters,

* E-mail: Scott.Kay@manchester.ac.uk

we quantify the difference and show that it can be as large as a factor of two, primarily due to the *clumpiness* in the ICM, associated with incomplete thermal support. We also show that the temperature directly derived from SZ data is the more faithful tracer of the underlying cluster potential, being within 10 per cent of the virial temperature in all clusters studied.

2 MEASURING CLUSTER TEMPERATURES

The temperature of the ICM (or any portion of it) is most easily measured by fitting a single-temperature plasma model to the observed X-ray spectrum. As the emission is primarily due to thermal bremsstrahlung (free-free) in hot clusters ($kT > 2$ keV or so), the temperature is determined by the energy scale, $E \simeq kT$, above which the emission decays exponentially. Since a single-temperature model is used to fit a multi-temperature distribution, the result is known as a spectroscopically-weighted average of the plasma temperature.

Recently, Mazzotta et al. (2004) calibrated this weighting using N -body/hydrodynamic simulations of galaxy clusters and proposed a simple estimator, known as the *spectroscopic-like* temperature

$$T_{\text{sl}} = \frac{\int \rho^2 T^{1/4} dV}{\int \rho^2 T^{-3/4} dV}, \quad (1)$$

where ρ is the mass density of a fluid element in volume, dV , with temperature, T . Since the weighting factor is $w = \rho^2 T^{-3/4}$, cooler dense (i.e. lower entropy) gas is weighted the most. Naturally, cooling gas increases its density to try and re-establish hydrostatic equilibrium, so regions where cooling is important (particularly the core) have a strong influence on the X-ray temperature of the ICM.

An alternative, but much harder, measurement of the ICM temperature comes from the spectral distortion induced by a cluster on the CMB, the SZ effect. The fractional change in CMB temperature is

$$\frac{\Delta T}{T_{\text{CMB}}} = \int \left[g(x) \frac{kT_e}{m_e c^2} + f(x, T_e) \frac{kT_e}{m_e c^2} + h(x) \frac{v_l}{c} \right] d\tau, \quad (2)$$

where $T_{\text{CMB}} = 2.725\text{K}$ (Mather et al. 1999), T_e is the electron temperature of the ICM, n_e its density, v_l the line-of-sight velocity, and $d\tau = n_e \sigma_T dl$ the change in optical depth to Compton scattering along the differential line element, dl . The three frequency-dependent pre-factors, $g(x)$, $f(x, T_e)$, $h(x)$, where $x = h\nu/kT_{\text{CMB}}$, allow the separation of the SZ signal to be performed (with $f(x, 0) = 0$ for all x).

The first term in equation (2) dominates for reasonable assumptions of cluster properties, and is due to the thermal energy of the (mainly) non-relativistic electron population. The second term is the temperature-dependent correction due to relativistic electrons which can be significant for hot clusters; it is this term that we will make use of to estimate the ICM temperature. Finally, the third term (known as the kinetic SZ effect) is due to the bulk motion of the plasma.

The frequency-independent part of the first term is usually expressed as the Compton y parameter

$$y = \int \frac{kT_e}{m_e c^2} d\tau. \quad (3)$$

Table 1. Weights used to define the hot ($T > 10^5\text{K}$) gas mass-weighted temperature, T_{mw} , the X-ray spectroscopic-like temperature, T_{sl} , and the SZ temperature, T_{SZ} .

Temperature	Weight
T_{mw}	$w = \rho$
T_{sl}	$w = \rho^2 T^{-3/4}$
T_{SZ}	$w = \rho T$

Following Hansen (2004), we can then define the Compton-average of any quantity F as

$$\langle F \rangle = \frac{1}{y} \int F \frac{kT_e}{m_e c^2} d\tau, \quad (4)$$

so the Compton-averaged electron temperature is

$$\langle T_e \rangle = \frac{1}{y} \int T_e \frac{kT_e}{m_e c^2} d\tau. \quad (5)$$

The relativistic correction, $f(x, T_e)$, can be approximated as $f(x, T_e) = T_e \delta(x)$; higher-order corrections due to ultra-relativistic electrons are subdominant in all but the very hottest clusters (Diego, Hansen & Silk 2003; Hansen 2004). In the Rayleigh-Jeans limit ($x \ll 1$), $g(x) = -2$ and $\delta(x) = 17k/5m_e c^2$ (Challinor & Lasenby 1998). Also ignoring the kinetic SZ effect, we can thus approximate equation (2) as

$$\frac{\Delta T}{T_{\text{CMB}}} = y[g(x) + \delta(x) \langle T_e \rangle]. \quad (6)$$

One can potentially extract $\langle T_e \rangle$ from multi-frequency SZ data, especially for hot $kT > 5\text{keV}$ clusters. This is a different average from the X-ray temperature, weighted instead by the gas pressure (so at a given density, the hottest, rather than coolest, gas is weighted highest). For simplicity, we will denote this temperature T_{SZ} in subsequent discussion. A summary of the weights used to define the gas temperatures is given in Table 1.

3 CLUSTER SIMULATIONS

We analyse N -body/hydrodynamic simulations of three galaxy clusters, selected from a larger sample already studied by Kay et al. (2004; hereafter K2004), to which we refer the reader for further details. The clusters were extracted from a large cosmological N -body simulation run by the Virgo Consortium,¹ and re-simulated at higher resolution and with gas using the GADGET2 code (Springel 2006). The clusters have similar masses [$M_{\text{vir}} = (1.0, 0.6, 0.9) \times 10^{15} h^{-1} M_{\odot}$] and radii [$R_{\text{vir}} = (2.0, 1.7, 2.0) h^{-1} \text{Mpc}$] at $z = 0$, but were chosen because they have significantly different merger histories (Powell et al., in preparation). While this sample is limited in size (primarily due to the amount of CPU time required), it nevertheless gives some indication of object-to-object variations on the scale of a typical rich cluster. Each cluster was re-simulated twice (see below), with $1 - 2 \times 10^6$ dark matter particles within R_{vir} (the dark matter and gas particle masses were $m_{\text{dark}} = 4 \times 10^8 h^{-1} M_{\odot}$

¹ <http://www.virgo.dur.ac.uk>

and $m_{\text{gas}} = 8 \times 10^7 h^{-1} M_{\odot}$ respectively). The force resolution (equivalent Plummer softening length) was fixed at $\epsilon = 10 h^{-1} \text{kpc}$ in comoving co-ordinates until $z = 1$, after which it was fixed at $\epsilon = 5 h^{-1} \text{kpc}$ in physical co-ordinates.

3.1 Cluster models

For each cluster, we considered two models for the gas physics, taking the total number of simulations performed to six. These models are very similar to those studied by K2004, so further details may be found there.

For the first model, labelled *non-radiative*, the gas was subjected to adiabatic forces and an artificial viscosity (to generate entropy in shocks) only. This was done using the standard SPH implementation in GADGET2 (Springel 2006). This model contains the minimum amount of physics required to model the formation of the ICM, being driven solely by gravitational processes. While a useful baseline, it does not match the observational properties of clusters.

For the second, more realistic, model, labelled *feedback*, the gas was subjected to the following additional processes. Firstly, gas particles with temperature $T > 10^4 \text{K}$ were able to cool radiatively, assuming a metallicity of $Z = 0.3 Z_{\odot}$. Second, gas that had cooled below $1.2 \times 10^4 \text{K}$ and reached hydrogen densities, $n_{\text{H}} > 10^{-3} \text{cm}^{-3}$, could either form stars (i.e. become collisionless) or be reheated to high temperature ($kT = 25 \text{keV}$), with equal probability (i.e. $f_{\text{heat}} = 0.5$ in the jargon of K2004). Tests revealed that the choice of density threshold and reheating temperature were necessary for the clusters to have sufficiently-high core entropy to lie on the $z = 0$ X-ray luminosity–temperature relation, while the choice of f_{heat} was primarily to produce a sensible cooled fraction (on average, only 14 per cent of the baryons within R_{500} had cooled by $z = 0$, similar to that observed by Lin, Mohr & Stanford 2003).

3.2 Estimating the temperatures from the simulations

The various 2D temperature distributions were computed from maps using the procedure outlined in Onuora, Kay & Thomas (2003). Briefly, the relevant weighting was computed for every hot ($T > 10^5 \text{K}$) gas particle within a cylinder of length $6R_{\text{vir}}$, and projected radius R_{vir} , centred on the cluster. These weightings were then smoothed, and projected along the length of the cylinder onto a 2D 800×800 pixel array using the projected version of the GADGET2 SPH kernel. Maps of the spectroscopic-like temperature, T_{sl} , were computed using the discrete version of equation (1) and the SZ temperature, T_{SZ} , using equation (5). For comparison, we also computed hot gas mass-weighted temperature maps (where the weight in equation (1) is replaced by $w = \rho$; see Table 1).

4 RESULTS

We first present various measurements of the mean temperature within the (projected) virial radius of each simulated cluster. Besides the X-ray and SZ temperatures, we also consider the projected hot gas mass-weighted temperature, T_{mw} , and the 3D virial temperature, T_{vir} (see

Table 2. Various temperature measurements (expressed as an energy, kT in keV units) within the virial radius. Column 1 gives the label for each simulation; column 2 the virial temperature; column 3 the hot gas mass-weighted temperature; column 4 the X-ray spectroscopic-like temperature; column 5 the SZ Compton-weighted temperature and column 6 the ratio of the SZ to X-ray temperatures. Values in brackets denote the ratio of each temperature to the virial temperature.

Cluster	kT_{vir}	kT_{mw}	kT_{sl}	kT_{SZ}	$T_{\text{SZ}}/T_{\text{sl}}$
NR1	5.7	4.2 (0.7)	4.0 (0.7)	6.1 (1.1)	1.5
NR2	4.0	2.7 (0.7)	2.2 (0.6)	3.9 (1.0)	1.8
NR3	6.0	3.8 (0.6)	2.7 (0.5)	5.6 (0.9)	2.1
FB1	5.3	4.4 (0.8)	5.4 (1.0)	5.9 (1.1)	1.1
FB2	3.9	3.3 (0.9)	3.5 (0.9)	4.4 (1.1)	1.2
FB3	6.2	4.5 (0.7)	4.8 (0.8)	6.2 (1.0)	1.3

Muanwong et al. 2002), the most suitable temperature for cosmological applications of clusters.

The measured temperatures² are given in Table 2. The hot gas mass-weighted temperature, T_{mw} , and X-ray spectroscopic-like temperature, T_{sl} , are both lower than the virial temperature, with the exception of one of the *feedback* clusters (FB1), where $T_{\text{sl}} \simeq T_{\text{vir}}$. In general, the difference between these two temperatures and the virial temperature is larger for the *non-radiative* clusters than the *feedback* clusters, the most extreme case being NR3, where $T_{\text{sl}} \simeq T_{\text{vir}}/2$. Part of this difference can be attributed to projection effects, i.e. including gas extending to 3 virial radii from the cluster centre, along the line of sight, when calculating T_{mw} and T_{sl} . Cooler gas, associated with infalling substructure, is more prevalent on the outskirts of clusters, causing a significant downward shift in the measured temperatures. When the calculation of projected temperatures is restricted to gas within R_{vir} in all directions, the difference between these temperatures and T_{vir} is approximately halved.

We also show, in Fig. 1 (top panel), how T_{sl} compares to T_{vir} when the former is measured within a projected radius $R < R_{\text{vir}}$ (as is the case with X-ray observations of clusters). Thus, the temperature at each value of R is a result of integrating over all gas within that radius. At R_{500} ($\sim R_{\text{vir}}/2$), the typical outer radius where T_{sl} can be reliably measured with high-quality X-ray data, T_{sl} is only slightly larger (within 10 per cent) than its value at R_{vir} . On the other hand, the SZ temperature, T_{SZ} , is higher than both T_{mw} and T_{sl} in all clusters studied and is much closer to T_{vir} (within 10 per cent). All clusters show that T_{SZ} converges to within 20 per cent of T_{vir} at $R > 0.6R_{\text{vir}}$ ($\sim R_{200}$). Finally, the ratio, $T_{\text{SZ}}/T_{\text{sl}}$ exhibits very different behaviour between the two models, but at small radius in particular, the SZ temperature can be significantly (tens of per cent) higher than the X-ray temperature. At the virial radius, one *non-radiative* cluster even has $T_{\text{SZ}} > 2T_{\text{sl}}$, a massive difference.

Figure 2 illustrates how the two temperatures (T_{sl} and

² In practical terms, the temperatures are at the lower end of what might be measurable through the SZ effect, but the overall results of this paper should not be significantly affected by using hotter clusters.

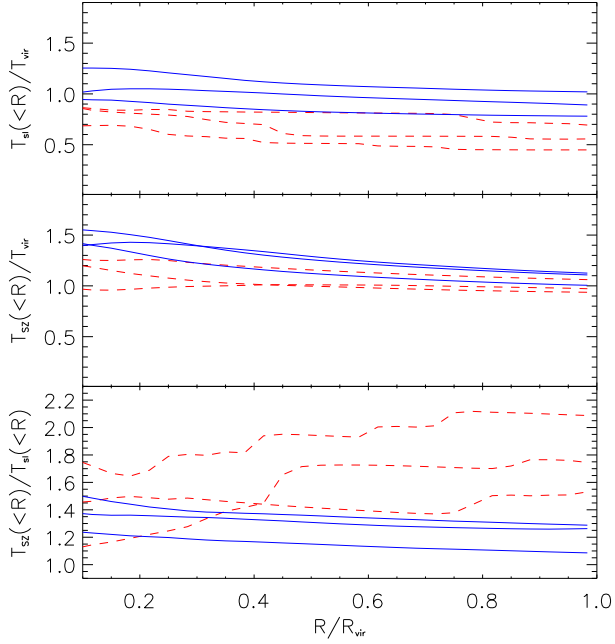


Figure 1. Mean temperature within a projected radius, R/R_{vir} , for the *non-radiative* (dashed lines) and *feedback* (solid lines) clusters. The top panel shows the (X-ray) spectroscopic-like temperature profiles, the middle panel the SZ temperature profiles (both panels show temperatures in relative to the virial temperature, T_{vir}) and the bottom panel the ratio of the two temperatures.

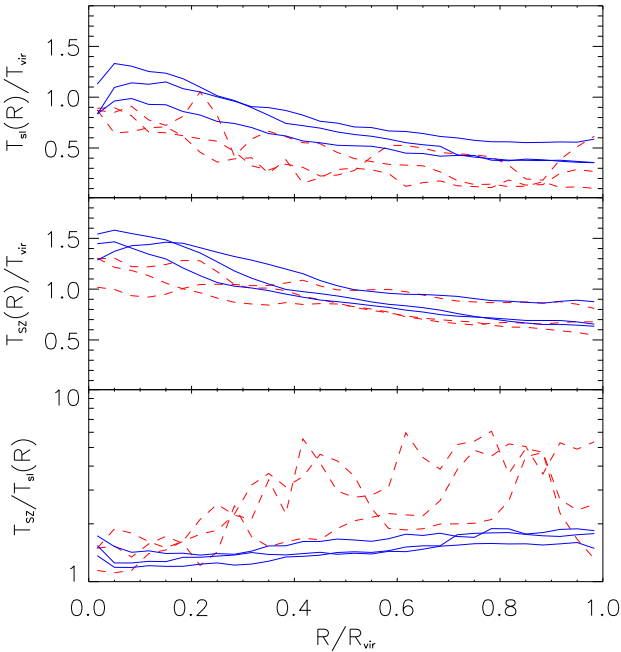


Figure 2. Azimuthally-averaged temperature profiles for the *non-radiative* (dashed lines) and *feedback* (solid lines) clusters. The top panel shows the (X-ray) spectroscopic-like temperature profiles, the middle panel the SZ temperature profiles and the bottom panel the ratio of the two temperatures.

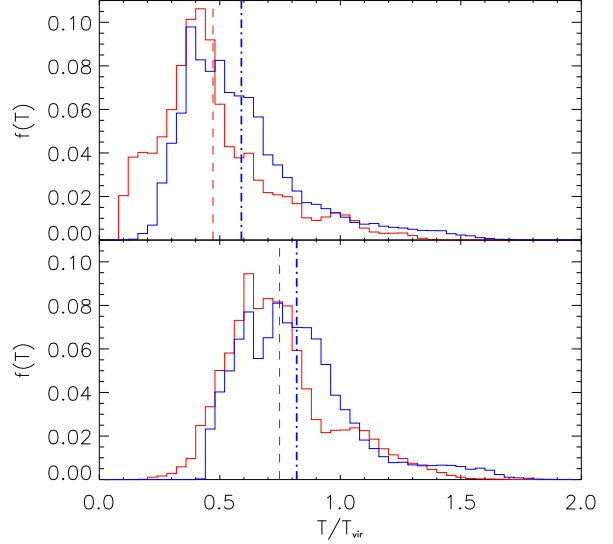


Figure 4. X-ray (top panel) and SZ (bottom panel) temperature distributions (fraction of pixels with a given T/T_{vir} value, within R_{vir}) for the *non-radiative* (thin lines) and *feedback* (thick lines) versions of cluster 1. Vertical dashed/dot-dashed lines illustrate the mean pixel value for the *non-radiative/feedback* models.

T_{SZ}) vary when measured locally, azimuthally-averaged at each radius. Strikingly, the SZ temperature profiles are very similar for both models outside $\sim 0.4R_{\text{vir}}$, suggesting that this estimator is insensitive to cluster physics away from the core. When the X-ray estimator is used, the *feedback* clusters are systematically hotter than the *non-radiative* clusters at all radii (except in the inner core, where a sharp drop occurs due to the presence of gas that has radiated a significant amount of its thermal energy). The bottom panel in the figure explicitly illustrates the ratio, $T_{\text{SZ}}/T_{\text{sl}}$, as a function of radius. In both models, the ratio increases with radius, although the effect is milder in the *feedback* clusters, with T_{SZ} almost a factor of two higher than T_{sl} at R_{vir} .

The reason why the SZ temperature is hotter than the X-ray temperature (and closer to the virial temperature) can be seen in Fig. 3, where we present maps of the two quantities (and their ratio) within R_{vir} for the first cluster (NR1 and FB1). In the *non-radiative* cluster, the map contains a significant amount of dark features, associated with infalling cooler, denser gas. Since T_{sl} weights this gas higher, they make a prominent contribution to the temperature of the cluster. Note that the nature of the cool gas changes in the *feedback* cluster. There it becomes more spot-like, associated with the cores of subhaloes; the combination of cooling and strong feedback has removed most of the cool, low-entropy, gas in this model. The difference in the amount of cool gas in the X-ray and SZ temperature maps is shown clearly in Fig. 4, where we plot pixel temperature distribution functions within R_{vir} . For the SZ distributions, the differences at the lowest temperatures are also much less significant.

5 SUMMARY

Our results clearly show that the temperature of the ICM, as measured through the SZ effect, can differ significantly from

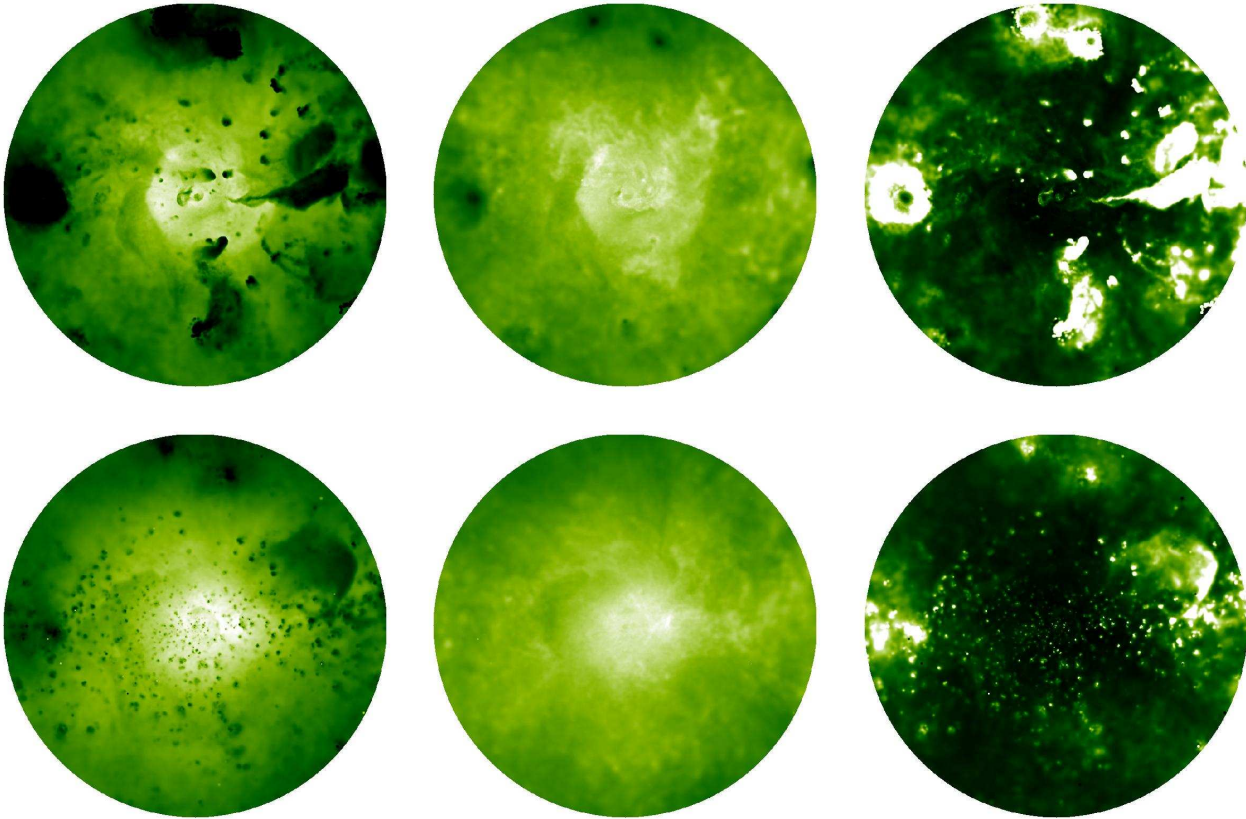


Figure 3. Maps of the *non-radiative* (top panels) and *feedback* (bottom panels) versions of cluster 1 within their virial radius ($2 h^{-1} \text{Mpc}$). From left to right: X-ray spectroscopic-like temperature, Compton-weighted SZ temperature and the ratio of the two. For the first two maps, the colour scale illustrates logarithmic temperature values, $\log(T/\text{K}) = [7, 8]$, while for the third, the scale illustrates ratios from 0 to 3.

the X-ray temperature of the cluster, with the SZ temperature always being the larger of the two. The X-ray temperature is weighted by cool dense gas the most, so differences between the amount of cool *clumpy* gas due to, for example, the level of radiative cooling and feedback, are most significant. On the other hand, the SZ temperature weights the hottest, densest gas (i.e. gas with the highest pressure) the most, so is generally a better estimator of the virial temperature of the cluster. Consequently, differences due to the amount of cooling and heating are less severe. The lower sensitivity of the SZ temperature to cluster physics (as compared to X-ray) is in line with previous comparisons between X-ray and SZ intensity (da Silva et al. 2001, 2004; Nagai 2006; Bonaldi et al. 2007).

In practice, the SZ temperature of a cluster is extremely difficult to measure, and its applicability limited to the hottest clusters, typically $kT > 5 \text{ keV}$. It does seem feasible, however, to design multi-wavelength experiments that are able to constrain SZ temperatures to $\sim 10 - 20$ per cent accuracy in the near future (Knox, Holder & Church 2004). Whether an instrument will ever be able to measure the SZ temperature in enough clusters, and to sufficient accuracy, to be useful for cosmological purposes (where the virial temperature is the desired quantity, c.f. Evrard et al. 2008) remains to be seen, but comparison with the X-ray temper-

ature of a cluster ought to provide useful information on the structure of the ICM.

ACKNOWLEDGEMENTS

We would like to thank the anonymous referee for their report that led to an improved version of this manuscript. We also thank Adrian Jenkins for generating the initial conditions for the simulations used in this paper and Mike Jones for useful discussions.

REFERENCES

- Ameglio S., Borgani S., Pierpaoli E., Dolag K., 2007, MNRAS, 382, 397
- Arnaud M., Pointecouteau E., Pratt G.W., 2005, A&A, 441, 893
- Bonaldi A., Tormen G., Dolag K., Moscardini L., 2007, MNRAS, 378, 1248
- Challinor A., Lasenby A., 1998, ApJ, 499, 1
- da Silva A.C., Kay S.T., Liddle A.R., Thomas P.A., Pearce F.R., Barbosa D., 2001, ApJ, 561, L15
- da Silva A.C., Kay S.T., Liddle A.R., Thomas P.A., 2004, MNRAS, 348, 1401
- Diego J.M., Hansen S.H., Silk J., 2003, MNRAS, 338, 796
- Evrard A.E., et al., 2008, ApJ, 672, 122

- Hansen S.H., 2004, MNRAS, 371, L5
- Itoh N., Kohyama Y., Nozawa S., 1998, ApJ, 502, 7
- Kay S.T., Thomas P.A., Jenkins A., Pearce F.R., 2004, MNRAS, 355, 1091 (K2004)
- Knox L., Holder G.P., Church S.E., 2004, ApJ, 612, 96
- Lin Y.-T., Mohr J.J., Stanford S.A., 2003, ApJ, 591, 749
- Mather J.C., Fixsen D.J., Shafer R.A., Mosier C., Wilkinson D.T., ApJ, 512, 511
- Mazzotta P., Rasia E., Moscardini L., Tormen G., 2004, MNRAS, 354, 10
- Muanwong O., Thomas P.A., Kay S.T., Pearce F.R., 2002, MNRAS, 336, 527
- Nagai D., 2006, ApJ, 650, 538
- Onuora L.I., Kay S.T., Thomas P.A., 2003, MNRAS, 341, 1246
- Pointecouteau E., Giard M., Barret D., 1998, A&A, 336, 44
- Pratt G.W., Böhringer H., Croston J.H., Arnaud M., Borgani S., Finoguenov A., Temple R.F., 2007, A&A, 461, 71
- Rephaeli Y., ARA&A, 33, 541
- Romer A.K., Viana P.T.P., Liddle A.R., Mann R.G., 2001, ApJ, 547, 594
- Ruhl J., et al., 2004, Proceedings of the SPIE, Volume 5498, pp. 11-29, The South Pole Telescope
- Springel V., 2006, MNRAS, 364, 1105
- Stanford S.A. et al. (the XCS Collaboration), 2006, ApJ, 646, L13
- Stebbins A., 1997, astro-ph/9709065
- Sunyaev R.A., Zel'dovich Y.B., 1972, Comments on Astrophysics and Space Physics, 4, 173
- Vikhlinin A., Markevitch M., Murray S. S., Jones C., Forman W., Van Speybroeck L., 2005, ApJ, 628, 655

This paper has been typeset from a \LaTeX file prepared by the author.